Wideband Single Pixel Radiometer in CMOS

van Berkel, S.L.; Malotaux, E.S.; Cavallo, D.; Spirito, M.; Neto, A.; Llombart, N.

DOI
10.1109/IRMMW-THz.2017.8067166

Publication date
2017

Document Version
Accepted author manuscript

Published in
42nd International Conference on Infrared, Millimeter, and Terahertz Waves, IRMMW-THz 2017

Wideband Single Pixel Radiometer in CMOS

S.L. van Berkel, E.S. Malotaux, D. Cavallo, M. Spirito, A. Neto and N. Llombart
Department of Microelectronics, TU Delft, The Netherlands

***Abstract*—The design and performance analysis are presented for a passive uncooled radiometer pixel suitable for integration in 28nm CMOS technology. In the configuration a single wideband antenna, operating from 200 GHz to 600 GHz, is connected to a pn-junction diode. Including the antenna-detector impedance mismatch, the detector shows an average NEP of $2.71\ pW/\sqrt{Hz}$ such that, together with the antenna, the radiometer promises fully passive and uncooled imaging capabilities with $2.6\ K$ temperature sensitivity at a $10\ Hz$ refresh rate. The design is planned for fabrication and measurement.**

I. Introduction and Background

Passive radiometers achieve the highest sensitivity and imaging speed when the detectors are cryogenically cooled [1], [2]. For the purpose of low-cost imaging applications cooling the system is undesirable. However, uncooled passive radiometers for millimeter wave imaging are limited in their sensitivity and thus their imaging speed by the electronic noise introduced by the detectors. Up to now CMOS integrated radiometers are not suitable for the purpose of low-cost real-time imaging applications; temperature sensitivities of uncooled passive radiometers have been shown above $2000K$ [3], [4]. The temperature sensitivity, ΔT, of a fully passive uncooled radiometer at a certain image refresh time, τ_i, can be shown to be [5]:

$$\Delta T = NEP/(k_B \Delta f_{RF}^{eff} \sqrt{\tau_i}) \tag{1}$$

where k_B is Boltzmann's constant, $\Delta f_{RF}^{eff} = \eta_{opt} \Delta f_{RF}$ is the effective bandwidth of the imager which includes the average system's optical efficiency η_{opt}. NEP is the noise equivalent power of the detector. As is clear from (1), the crucial aspect in achieving a practical NETD (e.g. $1\ K$ for security screening [6]) and imaging speed is the utilization of detectors characterized by a low NEP that are matched over a broad portion of the THz-spectrum to an antenna. Co-design of the antenna and detector is therefore a key point.

II. Radiometer Design

A schematic and simplified overview of the envisioned radiometer and the CMOS stratification are shown in Fig. 1(a) and Fig. 1(b) respectively (the CMOS stack is illustrated upside-down). The antenna is printed on the top metal layer of the CMOS stratification and radiates into the chip and through the low-resistivity silicon. The detector is a square-law detector implemented using a pn-junction diode. The detector is printed in the lower metal layers separated from the antenna by a thin SiO_2-substrate. The vias connecting the antenna and detector introduces an estimated parasitic inductance of $10\ pH$ and contains a capacitor of $25\ fF$ in order to block the DC-bias

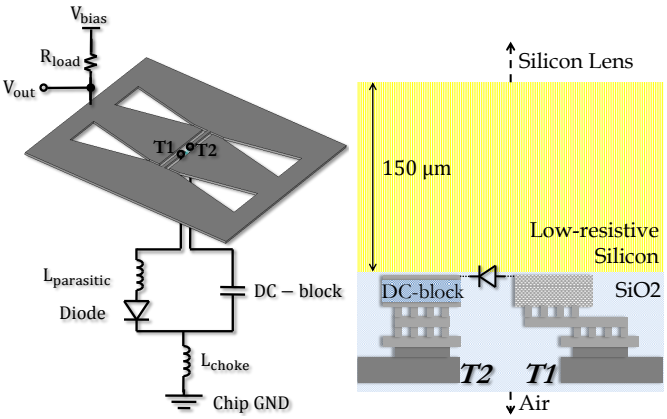

(a) Schematic Overview (b) CMOS Stratification

Fig. 1. Schematic of single-pixel radiometer

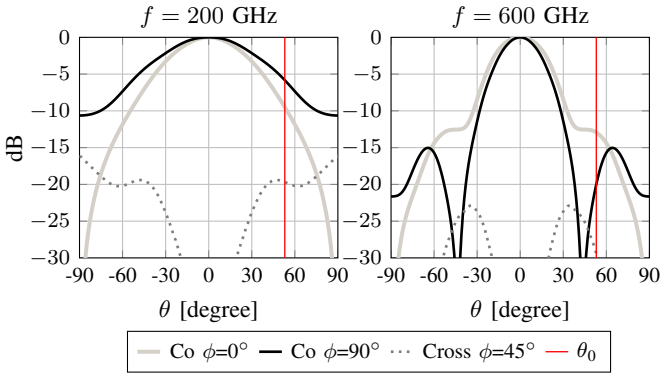

Fig. 2. Primary patterns (inside the lens) at 200 GHz and 600 GHz

voltage, V_{bias} (see Fig. 1(a)). The low-resistivity silicon of the technology is thinned down to $150\ \mu m$ and is directly attached to a silicon elliptical lens.

A. Antenna

The antenna is a double bow-tie slot [7] and in combination with an elliptical lens it operates like a leaky-lens [8] over a 1:3 relative frequency band from 200 GHz to 600 GHz. The elliptical lens is made of high-resistivity silicon with a matching layer ($\epsilon_r = 2.62$). The thin SiO_2-substrate introduces a leaky-wave behavior [8] enabling the 1:3 frequency band operation with clean patterns. The primary patterns, simulated on an infinite silicon substrate are as shown in Fig. 2 for 200 GHz and 600 GHz. Indicated by θ_0 is the truncation angle of the elliptical lens, $\theta_0 = 53°$. The aperture efficiency, η_{ape}, is shown in Fig. 3(a) which is defined as $\eta_{ape} = \eta_{tap}\eta_{opt}$,

where η_{tap} is the tapering efficiency on the lens and η_{opt} is the optical efficiency of the antenna. The optical efficiency includes the reflections and spill-over within the elliptical lens and ohmic losses in the SiO_2 and low-resistive silicon substrate. The average optical efficiency of the antenna feed over the operational bandwidth is $\eta_{opt} = 60.5\%$. The input impedance of the antenna, seen from the terminals *T1* and *T2* in Fig. 1(a) is shown by the solid lines in Fig. 3(b).

B. Detector

THz detectors suitable for CMOS integration that are commonly used are Schottky-diodes and MOSFETS. However, these devices are prone to high flicker noise (i.e. 1/f noise) contributions [9], [10]. A low 1/f corner frequency is desirable in order to be able to use large integration times (we focus on a 10 Hz refresh-rate, i.e. 0.1s available integration time) [11]. In this design we aim to use a pn-junction diode because such diodes are able to provide good voltage responsivity over the full operational bandwidth while simultaneously offering a low 1/f corner frequency [12]. Pn-junction devices are readily available and characterized in the available technology. The size of the diode and the DC-bias voltage impacts both the input impedance and responsivity of the diode. Therefore the choice in size and bias voltage implies a trade-off between the antenna-detector matching and the power-to-voltage conversion of the diode. The NEP follows from the simulated voltage responsivity and estimated white noise level v_n; $NEP = \frac{v_n}{R_v}$. The optimal NEP and voltage responsivity, including the antenna-detector mismatch, are shown respectively by the solid and dashed curves in Fig. 3(c) yielding $NEP = 2.71\ pW/\sqrt{Hz}$ and $R_v = 3.33\ kV/W$ averaged over the full bandwidth. The input impedance of the detector (including $L_{parasitic}$ and the DC-block in Fig. 1) seen from terminals *T1* and *T2* are shown by the dashed lines in Fig. 3(b) and results in the antenna-detector reflection coefficient as shown in Fig. 3(d).

III. Performance Analysis

With an average optical efficiency of $\eta_{opt} = 60.5\%$, the effective bandwidth of the antenna architecture is $\Delta f_{RF}^{eff} = 0.605 \cdot 400\ \text{GHz} = 242\ \text{GHz}$. Using (1) the sensitivity of the single pixel radiometer with a 10Hz refresh rate can be estimated to be $\Delta T = 2.6K$. A first single pixel prototype will be fabricated in order to demonstrate the potential sensitivity and validate the design steps.

Acknowledgements

This research is supported by the Dutch Technology Foundation STW (Project Terahertz silicon-Integrated CAMera for low-cost imaging applications, TiCAM, 13325), which is part of the Netherlands Organization for Scientific Research (NWO), and which is partly funded by the Ministry of Economic Affairs. N. Llombart would like to thank the European Research Council for the starting grant LAA-THz-CC (639749). The work of A. Neto was supported by European Research Council Consolidator Grant AAATSI (278794).

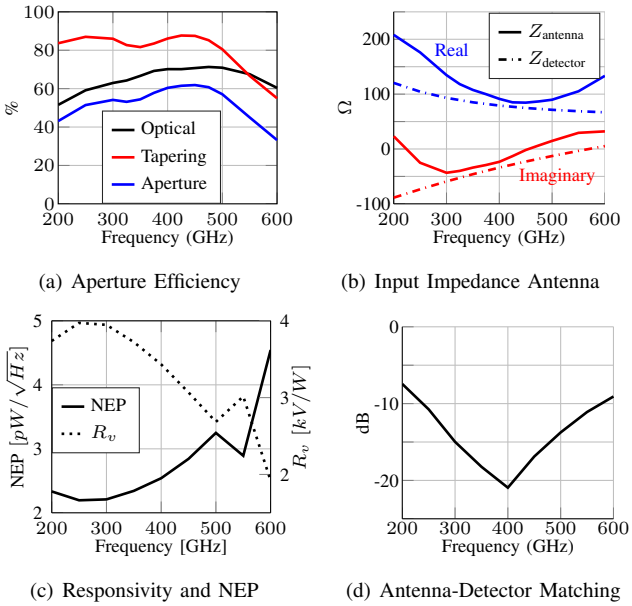

(a) Aperture Efficiency (b) Input Impedance Antenna

(c) Responsivity and NEP (d) Antenna-Detector Matching

Fig. 3. Antenna's aperture efficiency (a), Input impedance of both antenna and detector seen from terminals *T1* and *T2* in Fig. 1 (b), Simulated optimal NEP and responsivity including antenna-detector mismatch (c), Antenna-Detector mismatch at the terminals *T1* and *T2* in Fig. 1 (d).

References

[1] J. J. A. Baselmans, et.al., "A kilo-pixel imaging system for future space based far-infrared observatories using microwave kinetic inductance detectors," *A&A*, 2017.

[2] A. Timofeev, et.al., "Optical and electrical characterization of a large kinetic inductance bolometer focal plane array," *IEEE TST*, 2017.

[3] R. Hadi et. al., "A 1 k-Pixel Video Camera for 0.7-1.1 Terahertz Imaging Applications in 65-nm CMOS", IEEE JSSC 2012.

[4] S. Malz, et. al., "Towards passive imaging with CMOS THz cameras", Conference proceedings of IRMMW-THz 2016.

[5] A. Luukanen, et al., "Millimeter-wave and terahertz imaging in security applications", Terahertz Spectroscopy and Imaging 2012.

[6] C. Dietlein, et.al., "Phenomenology of passive broadband terahertz images," in *4th ESA Workshop on Millimetre-wave Technology and Applications*, 2006.

[7] A. J. Alazemi, et. al., "Double Bow-Tie Slot Antennas for Wideband Millimeter-Wave and Terahertz Applications", IEEE TST 2016.

[8] A. Neto, "UWB, non dispersive radiation from the planarly fed leaky lens antenna Part 1: Theory and design", IEEE TAP 2010.

[9] D. Kim, et. al., "Design and Demonstration of 820-GHz Array Using Diode-Connected NMOS Transistors in 130-nm CMOS for Active Imaging", IEEE TST 2016.

[10] R. Han, et. al., "Active Terahertz Imaging Using Schottky Diodes in CMOS: Array and 860-GHz Pixel", IEEE JSSC 2013.

[11] J. Lesurf, "Information and measurement", CRC press 2001.

[12] Z. Ahmad, et.al., "THz Detection Using p^+/n-Well Diodes Fabricated in 45-nm CMOS", IEEE EDL 2016.